Intermediate layer free PVDF evolved CMS on ceramic hollow fiber membrane for CO2 capture

Intermediate Layer Free PVDF Evolved CMS on Ceramic Hollow Fiber Membrane for CO_2 Capture

Yen-Hsun Chen[a], Po-Chun Wu[a], Joy Thomas[b], Hsiang-Yu Wang[a], Guo-Liang Zhuang[a,d], Zhen Wang[a], Hui-Hsin Tseng[d], Dun-Yen Kang[a], Cheng-Liang Liu[b,c], Kuo-Lun Tung[a,c,e*]

[a] Department of Chemical Engineering, National Taiwan University, Taipei 106, Taiwan

[b] Department of Materials Science and Engineering, National Taiwan University, Taipei 106, Taiwan

[c] Advanced Research Center for Green Materials Science and Technology, National Taiwan University, Taipei 106, Taiwan

[d] Department of Environmental Engineering, National Chung Hsing University, Taichung, 402, Taiwan

[e] Water Innovation, Low Carbon and Environmental Sustainability Research Center (WInnER Center), National Taiwan University, Taipei, 10617, Taiwan

***Corresponding author**Prof. Kuo-Lun Tung

Tel: +886-2-3366-3027; Fax: +886-2-2362-3040; Email: kltung@ntu.edu.tw

Highlights:

- Intermediate layer free growth of uniform CMS over the ceramic hollow membrane
- Controlled PVDF concentration with homogenous pore hollow support provides defect-free membrane
- PVDF originated CMS prescribes higher molecular precision for CO_2 capture
- PVDF based CMS enhances the resilience towards aging for the carbon separation
- Robust CMS membranes can advertise enhances carbon capture for a month duration

Abstract

The use of carbonized polymers has ushered in a new class of materials with profound implications for the gas separation industry. This study explored the transformation of polyvinylidene fluoride (PVDF) into microporous carbon structures coated onto ceramic substrates, enabling in situ growth of carbon molecular sieve (CMS) materials over hollow fibers. This material featured more robust CMS membranes than alumina and demonstrated exceptional capability in vital gas separations, particularly for CO_2/CH_4. This novel approach increased the selectivity for gases and exhibited remarkable aging resilience, so the material is a compelling candidate for high-performance gas separations. Furthermore, after 31 days, the weathered carbon dioxide membrane exhibited a slight permeability drift from 234.88 barrers to 195.35 barrers, while the CO_2/CH_4 ratio increased from 24.21 to 57.14, surpassing the Robeson 2008 upper bound. The PVDF-derived supported hollow fiber carbon membranes provide a blueprint for designing membranes for carbon capture. With the high packing density of the hollow fiber membrane and improved mechanical strength of the supported carbon membrane, this approach overcame the high fabrication costs and brittleness of other carbon membranes. In addition, the entire process for preparation of the PVDF carbon films is easily scaled up and has great potential for future practical application.

Keywords: PVDF-derived carbon membrane, hollow fiber carbon membrane, carbon capture, aging-resilience

1. Introduction

Gas separation plays a pivotal role in various industrial processes, particularly in the oil and gas, petrochemicals, and environmental conservation sectors [1, 2]. The significance lies in its ability to separate and purify different gases, allowing for extraction of the valuable components, removal of impurities, and meeting stringent quality standards. In the oil and gas industry, gas separation is essential for separating methane, ethane, propane, and other gases from natural gas streams [3]. These separated gases have different uses and values, so efficient separation is economically crucial. Gas separation enables production of the high-purity gases vital for chemical processes. Separating and capturing greenhouse gases such as carbon dioxide (CO_2) are critical for mitigating climate change and reducing the emissions from industrial processes [4-6]. Polymer membranes constitute a significant area of research in gas separations due to their potential for cost-effective and energy-efficient separation processes [7, 8]. However, several challenges and crises persist in this field [9, 10]. One of the significant challenges is managing the trade-off between permeability and selectivity, making it complex to achieve optimal performance. Another critical challenge is improving the thermal resistance and durability. Membranes must withstand high temperature and be stable for a long time since the membranes are usually operated at higher temperature. Furthermore, scaling up production to industrial scale presents several challenges, including maintaining consistent quality, ensuring cost-effectiveness, and overcoming technical barriers associated with large-scale manufacturing processes. Overcoming these challenges requires interdisciplinary research combining materials science, polymer chemistry, engineering, and computational modeling. To address these limitations and increase the capabilities of polymer membranes in gas separations,

scientists are continually exploring new polymer compositions, surface modifications, advanced characterization techniques, and innovative manufacturing processes.

Carbon molecular sieve (CMS) membranes are promising candidates for efficient gas separations owing to their unique structures and gas transport properties [11, 12]. The tunability of CMS membranes derived from polymer precursors present a promising avenue for overcoming the inherent limitations and optimizing gas separation processes [13-17]. This research explored the benefits and recent research endeavors focused on tailoring polymer precursors to achieve enhanced selectivity, permeability, and stability in CMS membranes [18-21].

The selection and modification of polymer precursors play pivotal roles in determining the structural and transport properties of CMS membranes. Various strategies, including polymer blending, cross-linking, functionalization, and templating, have been employed to fine-tune the pore structures and surface chemistry of CMS membranes [22-25]. These approaches enable control of the pore size distribution, surface functionality, and structural integrity, thereby influencing the gas separation performance [26, 27]. There are extensive reports of fabricating carbon membranes using cellulose [28], polyimide (PI) [29-31], polyetherimide (PEI) [32, 33], poly(furfuryl alcohol) (PFA) [34], polyvinylidene chloride (PVDC) [35, 36], polymers of intrinsic microporosity (PIM) [37], polybenzimidazole (PBI) [38], phenol formaldehyde [39], polyacrylonitrile (PAN) [40] and so on. However, few studies have used PVDF as a precursor to fabricate CMSs. PVDF can be synthesized easily due to its simple structure, so it is much less expensive than other precursors. Furthermore, PVDF has a lower decomposition temperature than other common precursors, indicating that the PVDF CMS fabrication process requires less energy for pyrolysis

[41]. These advantages provide an opportunity to commercialize PVDF CMSs.

In this work, homemade macroporous alumina hollow fibers were used as the substrate, and the raw material PVDF was chosen as the polymer precursor. The PVDF-derived carbon molecular sieve membrane (CMSM) was fabricated by direct dip-coating only once without coating an intermediate layer due to good adhesion between the PVDF and alumina hollow fiber substrate.

2. Experimental

2.1. Materials

The chemicals used for the ceramic hollow fiber membrane included Aluminum oxide, α-phase was purchased from Alfa Aesar, N-Methyl-2-pyrrolidone (NMP) from Choneye Pure Chemicals, Polyethersulfone(PES) from Solvay Trump Chemical, Polyethyleneglycol 30-dipolyhydroxystearate (P135) from Croda Taiwan. The chemicals used for Poly(Vinylidene Fluoride) Membrane included Poly(vinylidene fluoride) (PVDF) was purchased from Alfa Aesar, N-N-Dimethylacetamide (DMAc) from Alfa Aesar.

2.2. Preparation of PVDF-derived CMSMs

The alumina hollow fiber was fabricated according to our previous study [42]. PVDF-derived CMSMs were prepared using the dip-coating method without coating an intermediate layer, followed by controlling the concentration of polymer solution and the pyrolysis parameters under the inert condition. The PVDF precursors were dissolved in DMAc and stirred at 300 rpm at 60^{o}C for at least 12 hr to make 5, 10, and

15wt% PVDF solution. The PVDF solution then was dip-coated directly only once onto the shell side of ceramic hollow fibers, which was sealed with epoxy resin before, at a speed of immersion of 5 mm/s and a speed of withdrawal of 1mm/s. The retention time was 20s. After the dip-coating process, the as-coated ceramic hollow fibers were kept on the dip coater for 3 minutes and then were dried at 110°C under vacuum for 4 hr to remove any water trapped in the as-coated ceramic hollow fibers.

The pyrolysis system is shown in Fig. 1, and the heating protocol is shown in Fig. S1. The as-coated ceramic hollow fibers were placed in the crucible and loaded in a quartz tube. Before the start of each pyrolysis, the quartz tube was vacuumed at 1×10^{-2} torr for at least 20 min. Then the quartz tube was purged with 99.999% nitrogen at the 200 cc/min flow rate to remove any oxygen or other gases until the pyrolysis process finished. The as-coated ceramic hollow fibers were first heated from 25°C to 250°C at a ramp rate of 10.0°C/min to reach polymer oxidative stabilization, preventing structure decomposition after pyrolysis. Next, temperature continuously rose to $(T_p - 15)$°C at a ramp rate of 3.85°C/min, where T_p is the final pyrolysis temperature ranging from 500°C to 600°C. Then as-coated ceramic hollow fibers were heated slowly from $(T_p - 15)$°C to T_p at a ramp rate of 0.25°C/min and the thermal soaking time was controlled at 2 hr. After pyrolysis, as-coated ceramic hollow fibers were cooled naturally to room temperature and the PVDF-derived CMSMs were obtained. The regeneration process of aged CMS membranes was heating the membrane using the aforementioned procedure. PVDF-derived CMSM was labeled CMS_X_Y, where X is the concentration of PVDF solution (5%, 10%, and 15%), and Y is the final pyrolysis temperature (500°C, 550°C, and 600°C).

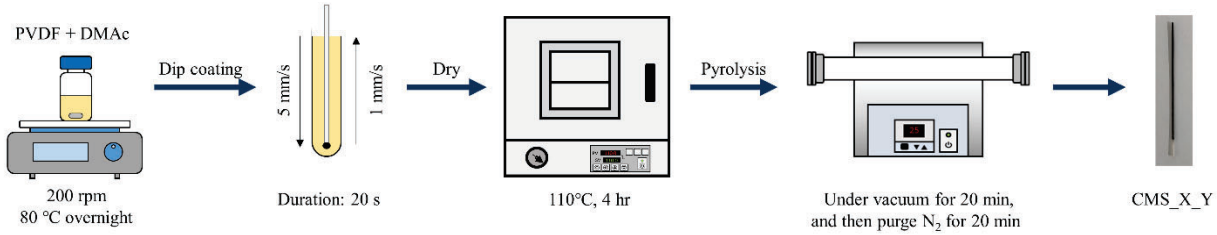

Fig. 1. The schematic illustration of the process of membrane preparation.

2.2. Membrane Characterization

The morphological studies and chemical element analyses of the samples were carried out with field emission scanning electron microscopy (FE-SEM, Nova^{TM} NanoSEM 230, FEI, USA) equipped with energy-dispersive spectroscopy (EDS). Average Pore size and pore size distribution are measured with the Capillary Flow Porometer (CFP, MMN-GL1500AE, Porous Measurement Int'l Ltd, Taiwan). Thermogravimetric Analysis (TGA, Pyris 1, PerkinElmer) is a technique to provide physical phenomena and chemical phenomena by monitoring the sample's mass loss during the heating process under a controlled atmosphere and comparing the relationship between weight loss, temperature and time, the samples were heated from 50ºC to 800ºC under nitrogen at a rate of 10ºC/min. Raman spectroscopy (NRS-5000, JASCO) can provide information on the crystal structure, electronic structure and lattice vibration of material. The surface roughness was measured with an atomic force microscope (Innova AFM, Bruker) using a probe (PPP-RTNCHR-50, Nanosensors) with a frequency of 330 kHz and a force constant of 42 N/m. The functional groups of the samples were characterized by attenuated total reflectance Fourier transform infrared spectroscopy (ATR-FT-IR, Perkin Elmer Spectrum 100) over the range 4000–500 cm^{-1}. The membrane surface element compositions were confirmed by X-ray

176 photoelectron spectroscopy (XPS-ESCA, VG Scientific ESCALAB 250).

177

178 *2.3. Gas separation test*

179 The schematic illustration of the constant pressure gas permeation system is shown
180 in Fig. S2. The sample to be tested was sealed with epoxy resin and fixed in the stainless
181 module. Before each gas permeation test, the upstream and the downstream were
182 vacuumed by a vacuum pump to remove the test gas remaining from last gas permeation
183 test. The kinetic diameters of the tested gas are CH_4 (3.80 Å) > N_2 (3.64 Å) > CO_2
184 (3.33Å). However, each test was performed in the order of N_2, CH_4, and CO_2, not
185 following the kinetic diameters since CO_2 is a condensable gas molecule compared to
186 other tested gases. The condensable property may reduce the next tested gas permeation
187 performance due to the absorbance of gas molecules on the membrane's pores.

188 The constant pressure/variable volume method was applied for all the single gas
189 permeation tests. The upstream constant gauge pressure was about 2 bar, and the
190 module was kept at room temperature. The results of this research are the average of
191 triplicate from different batches.

192 The gas permeability (P) was calculated from the equation 1:

193 $$\mathrm{P\ (barrers)} = 10^{-10} \times \frac{Q \cdot l}{\Delta p \cdot A} \quad \text{(Eq. 1)}$$

194

195 where Q is the gas flux (cm^3/s), l is the thickness of the membrane measured in
196 cm, Δp is the constant transmembrane pressure measured in cmHg, and A is the
197 effective membrane area in cm^2. Ideal selectivity (α) was calculated from the equation
198 2:

199 $$\alpha = \frac{P_a}{P_b} \quad \text{(Eq. 2)}$$

where P_a and P_b represent the permeability of gases species a and b, respectively.

The mixed gas tests were conducted in constant volume/variable pressure method. In mixed gas tests, the feed gas was composed of CO_2/CH_4 (50/50 mol%) at a total pressure of 2 bar at 25ºC. The gas composition was measured by gas chromatography (Shimadzu GC-2030) with a thermal conductivity detector. The permeability was computed by equation (1) in single gas test, and the selectivity was calculated using the following equation:

$$\alpha_{a/b} = \frac{y_a/y_b}{x_a/x_b}$$

where x_a and y_a are the molar fraction of gas a in the feed side and permeate side, respectively; x_b and y_b are the molar fraction of gas b in the feed side and permeate side, respectively.

3. Results and Discussion

3.1. Effect of the Concentration of the PVDF Solution

Initially, 5, 10, and 15 wt% PVDF solutions were prepared for the dip-coating process. Then, the as-coated membrane was pyrolyzed to fabricate PVDF-derived CMSMs. The effect of the PVDF concentration on the quality of the coating layer and the relationship between the coating solution concentration and gas permeation of the CMSMs will be discussed.

The XRD pattern for the self-standing PVDF-derived CMSMs is shown in **Error! Reference source not found.** S3. Broad peaks were observed in all spectra, exhibiting

223 the amorphous structures of the pyrolyzed CMS samples. As the concentration of the
224 PVDF solution increased, the 2θ (d002) peak shifted from 21.5° to 22.3°, indicating that
225 the d-spacing decreased. That is, the PVDF-derived CMSMs were prepared with higher
226 concentrations of PVDF solution and identical pyrolysis treatments, suggesting a more
227 densely packed structure due to smaller spacing between the individual polymer chains
228 in the PVDF solution. The average spacing between neighboring carbon atoms within
229 graphene planes was determined with the 2θ peak at approximately 43°, with a d-
230 spacing of 2.1 Å corresponding to the d100 plane in the graphite lattice [43].

231 As shown in Fig. S4 and Fig. S5, alumina hollow fibers with inner and outer
232 diameters of 0.85 mm and 1.30 mm, respectively, were fabricated, and the average pore
233 size was 261 nm. The surface and cross-sectional images of the PVDF-derived CMSMs
234 are shown in Fig. 2. There was no apparent dense carbon layer on the surface or cross-
235 section of the CMS_5_500 SEM image, as shown in Fig. 2(a1)(b1). Since the viscosity
236 of the 5 wt% PVDF solution was low and the substrate was macroporous, the 5 wt%
237 PVDF solution easily penetrated the substrate and was not trapped in the substrate. The
238 concentrated solution had fewer mobile polymer chains due to strong entanglement [44].
239 Thus, it was difficult for the highly entangled polymeric solution to penetrate the
240 substrate pores to form a good mechanically interlocking layer. In contrast to
241 CMS_5_500, the interlocking depths of CMS_10_500 and CMS_15_500 were
242 approximately 7.7 and 4.7 μm, respectively, and they exhibited dense and defect-free
243 layers, as shown in **Error! Reference source not found.**Fig. 2(b2) and (b3), due to the
244 presence of sufficiently mobile polymer chains and better adhesion between the
245 substrate and the casting solution, which was enhanced by the strong hydrogen bonds
246 formed between the abundant -OH groups on the substrate surface and the fluorides in

the PVDF.

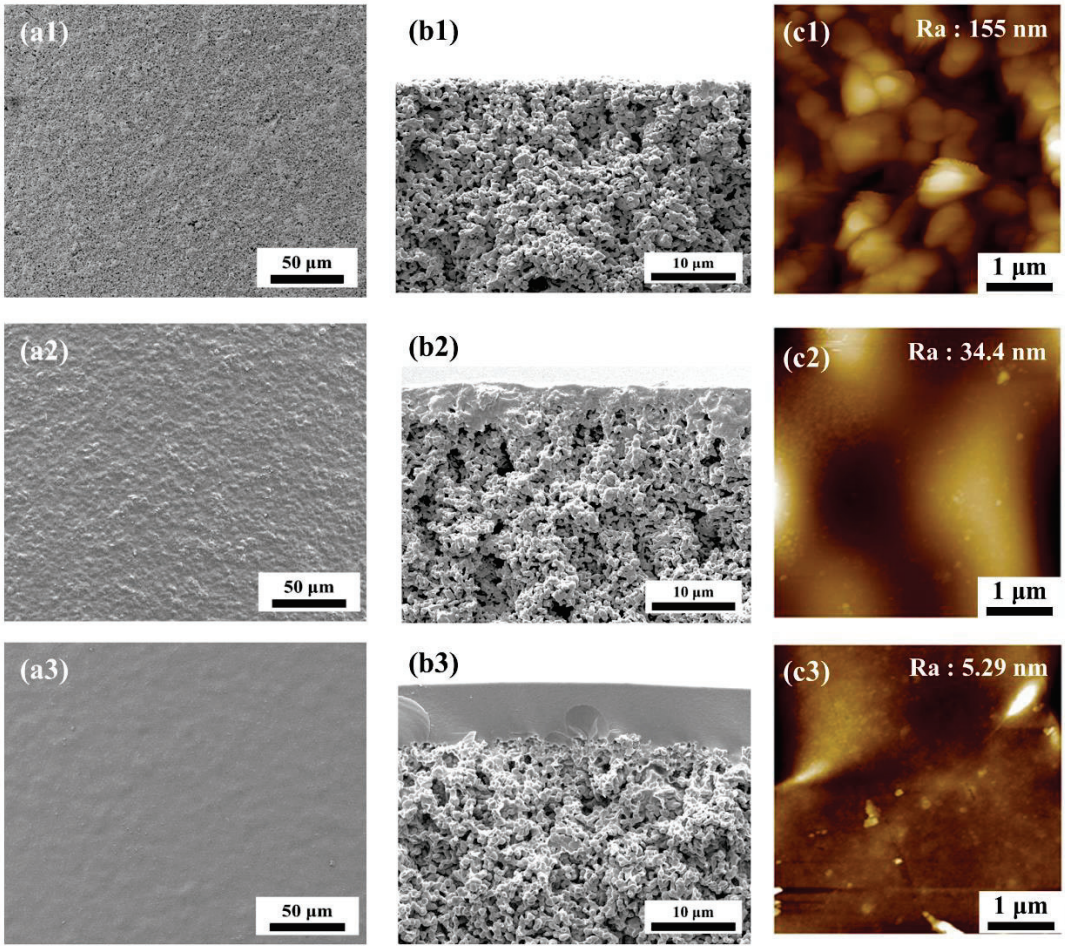

Fig. 2. (a) SEM images of outer surface morphology, and (b) SEM cross-section images (c) AFM images of PVDF-derived CMSMs prepared by (1) 5 wt%, (2) 10 wt%, and (3) 15 wt%, respectively.

The roughness and topographies of the PVDF-derived CMSMs are shown in Fig. 2(c). The roughness of CMS_5_500, CMS_10_500 and CMS_15_500 were 155 nm, 34.4 nm and 5.29 nm, respectively. CMS_15_500 had the smoothest carbon layer due to the appropriate viscosity of the PVDF solution coating the substrate. However, although CMS_10_500 was thinner than CMS_15_500, it led to the formation of a rougher carbon layer surface. After the pyrolysis process, a few carbon compounds

formed on the outer surface of the alumina particles, which increased the roughness. The AFM analysis was consistent with the SEM images. A smooth carbon layer was successfully fabricated without an intermediate layer.

Fig. 3 shows the gas separation performance and thickness of the as-prepared CMSMs fabricated from polymer solutions with different concentrations. The results are shown in Table S1. The gas permeances of CMS_5_500 for all tested gases were extremely high due to failure of the carbon separation layer, and the permeances all decreased in the order CH_4 (16 Dalton) > N_2 (28 Dalton) > CO_2 (44 Dalton). The gas permeance of CMS_10_500 and CMS_15_500 decreased in the order CO_2 (0.33 Å) > N_2 (3.64 Å) > CH_4 (3.80 Å). The permeance of nitrogen was greater than that of methane, indicating molecular sieving.

CMS_10_500 had a thinner carbon layer than CMS_15_500 and exhibited a lower gas resistance, but CMS_15_500 was fabricated with a higher concentration of PVDF, and more pores were formed with more PVDF precursors. Therefore, CMS_15_500 had more pores available for gas permeation. Thus, the gas permeances of CMS_10_500 for all tested gases were only slightly greater than those of CMS_15_500. Nevertheless, CMS_10_500 had lower selectivity for CO_2/N_2 (13.7) and CO_2/CH_4 (15.6) due to the larger d-spacing of CMS_10_500 (4.05Å). Compared to CMS_10_500, CMS_15_500 (3.98Å) had a more densely packed carbon structure, leading to the highest selectivity for CO_2/N_2 (15.2) and CO_2/CH_4 (16.1).

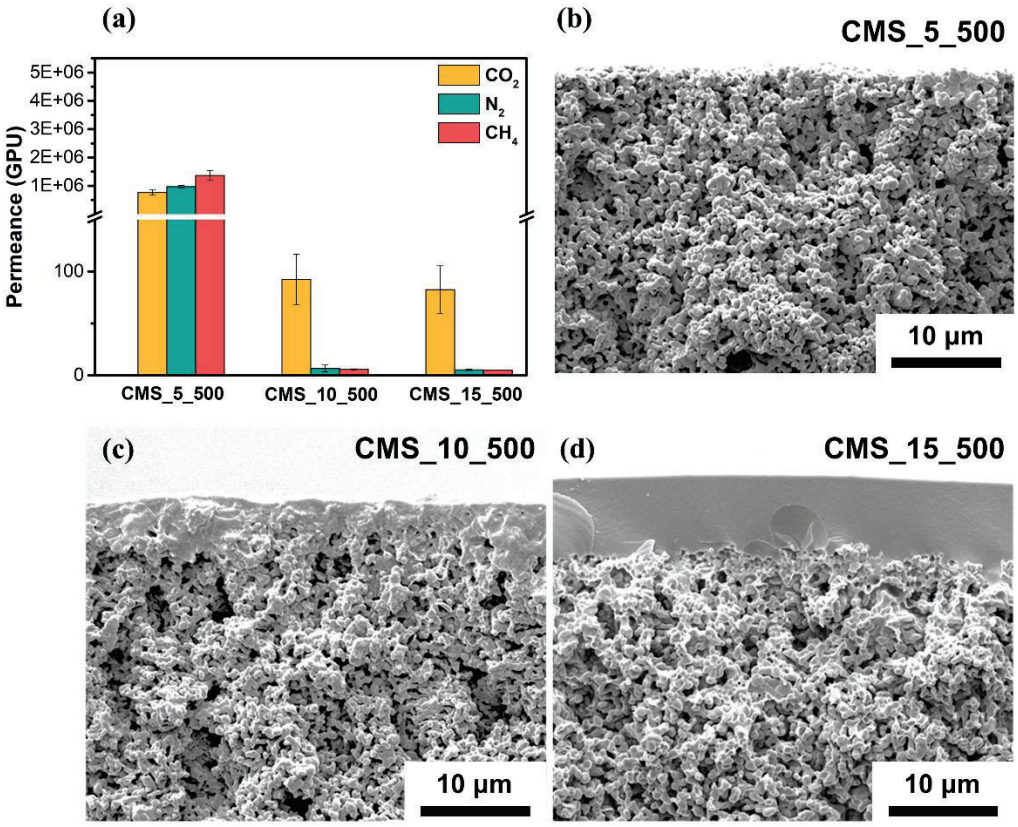

279

280 Fig. 3. (a) The gas permeance of PVDF-derived CMSMs prepared with the different
281 concentration of PVDF solution. (b)(c)(d) The cross-section SEM images of the
282 membranes.

283

284 *3.2 Effect of The Pyrolysis Temperature*

285 The TGA results for the neat PVDF films are shown in Fig. S6. The PVDF films
286 were stable until the temperature was increased to 400 °C, and they started to
287 decompose above 400 °C [41]. From 500 °C to 800 °C, the degradation rate decreased,
288 indicating that a completely stable rigid carbon structure had gradually developed.
289 However, when the temperature was greater than 700 °C, the weight loss of the neat
290 PVDF film was too high, resulting in difficult defect-free CMSM fabrication. In this
291 study, the effects of the pyrolysis temperatures (T_p) were determined by adjusting the

292 T_p to 500 °C, 550 °C and 600 °C. The surface morphology and cross-sectional images
293 of the PVDF-derived CMSMs are shown in Fig. S7, which indicates that the outer
294 surfaces of the PVDF-derived CMSMs fabricated at different T_p were all dense, smooth
295 and defect-free. As the pyrolysis temperature increased from 500 ºC to 600 ºC, the
296 carbon separation layer reduced from 7.02 μm to 2.89 μm; influencing a deprivation
297 over selectivity. When T_p was increased, more chemical components decomposed to
298 construct a rigid carbon structure [45]. Thus, the thickness of the carbon separation
299 layer decreased as T_p was increased.

300 The XRD patterns of the self-standing PVDF-derived CMSMs fabricated at
301 different T_p are shown in Fig. 4(a). Three broad diffraction peaks indicated the
302 formation of amorphous carbon containing graphite-like basal planes. The interlayer
303 spacings (d002 values) of CMS_15_500, CMS_15_550 and CMS_15_600, which were
304 3.96 Å, 3.89 Å and 3.78 Å, respectively, revealed that more tightly packed carbon
305 structures formed when the T_p was greater. In addition, weak peaks at 2θ angles of
306 approximately 43° were observed for all CMSMs, indicating the formation of graphite-
307 like planes because the 2θ peaks at approximately 43° represented the spacings of the
308 d100 and d101 carbon planes on the graphite-like planes. As T_p increased, the 2θ peak
309 at approximately 43° became more intense, demonstrating that a higher pyrolysis
310 temperature resulted in the formation of more graphite-like planes.

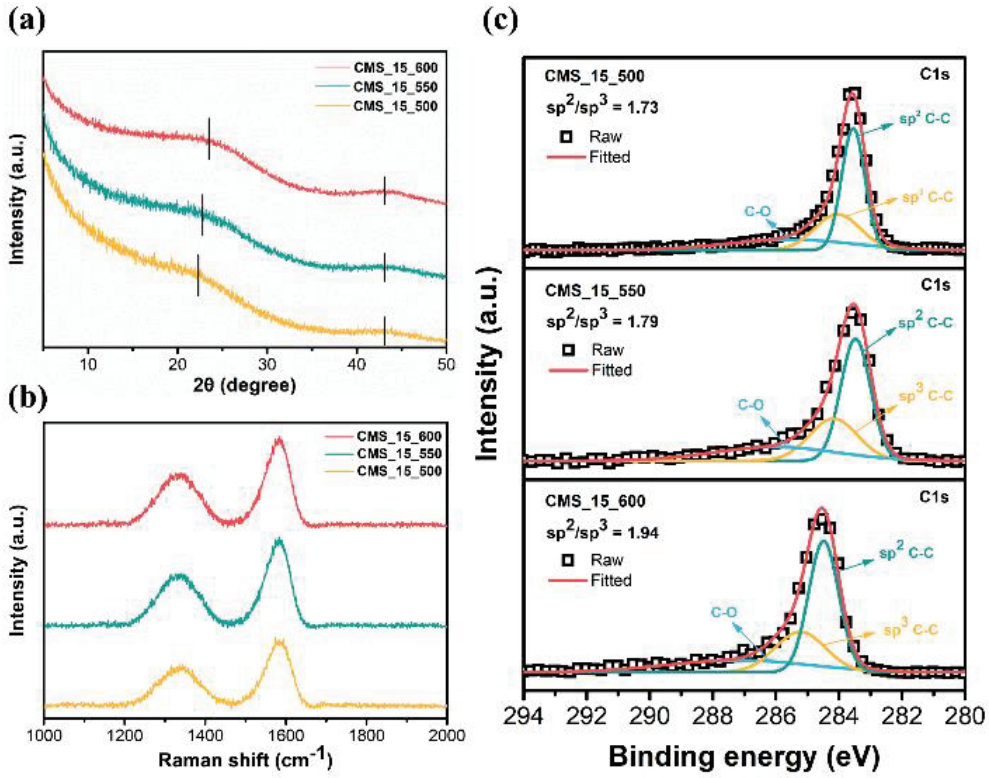

311

312 Fig. 4. (a) X-ray diffraction (b) Raman spectra (c) XPS patterns of the PVDF-derived

313 CMSMs prepared at different pyrolysis temperature.

314

315 Raman analysis is a valuable tool for detecting the graphitic plane orientations of

316 CMSMs. The Raman spectra of PVDF-derived CMSMs prepared with different

317 pyrolysis temperatures are shown in Fig. 4(b). The intensity ratios of the D-peak and

318 G-peak, which are referred to as I_D and I_G, respectively, are shown in Table S2. All of

319 the CMSMs exhibited two main peaks at approximately 1344 cm^{-1} and 1584 cm^{-1},

320 representing the D-peak and G-peak, respectively. The D-peak corresponds to the

321 defective structure of graphite, and the G-peak corresponds to the regular graphite

322 structure. Thus, the intensity ratio of the D-peak and G-peak (I_D/I_G) can be utilized to

323 identify the extent of orientation in the carbon surface microstructure [46]. As shown

in Table S2, the I_D/I_G ratio decreased from 0.64 to 0.58 as the pyrolysis temperature was decreased, indicating that the PVDF-derived CMSMs fabricated at higher temperatures had more ordered graphitic sp^2 carbon structures.

The XPS patterns of the three PVDF-derived CMSMs are shown in Fig. 4(c). The deconvoluted C 1s XPS spectrum confirmed the presence of an ordered graphitic sp2 carbon structure in the PVDF-derived CMSMs. In addition, the coexistence of sp2 and sp3 hybridized carbon was clearly observed, showing that the PVDF-derived CMSMs had amorphous and crystalline structures and confirming the existence of a bimodal pore size distribution [47]. Moreover, as the pyrolysis temperature was increased from 500 °C to 600 °C, the sp2/sp3 ratio increased from 1.73 to 1.94, indicating that a more ordered microstructure of the carbon membrane was produced. The tendency of the sp2/sp3 content was consistent with the Raman analysis.

The surface elemental compositions of the three PVDF-derived CMSMs are shown in Table S3. A greater proportion of C and lower contents of the other elements were observed for CMS_15_600. During the pyrolysis process, the chemical bonds of the PVDF precursor were broken, and volatile compounds were released, leading to the formation of rigid carbon bonds. Thus, the increased carbon content with decreasing contents of the noncarbon elements indicated more complete carbonization of the carbon membrane. That is, carbonization of CMS_15_500 was decreased due to the lower pyrolysis temperature.

Single gas permeation studies were conducted to determine the gas separation capabilities of the as-prepared CMSMs fabricated at different pyrolysis temperatures, and the results are shown in Fig. 5(a)(b) and Table S4. The permeability of CO_2, N_2 and

CH_4 for all PVDF-derived CMSMs decreased in the order CO_2 (0.33 Å) > N_2 (3.64 Å) > CH_4 (3.80 Å). Molecular sieving effects were indicated by the gas permeability results. That is, the permeability of nitrogen, which is smaller and had a lower critical temperature, was greater than that of methane due to the molecular sieving effects. In addition, there was a little fluorine in all of the CMSMs, and the high electronegativity of fluorine enhanced the molecular interactions between polar molecules such as CO_2 and the carbon structure, which increased the permeability of CO_2 [48].

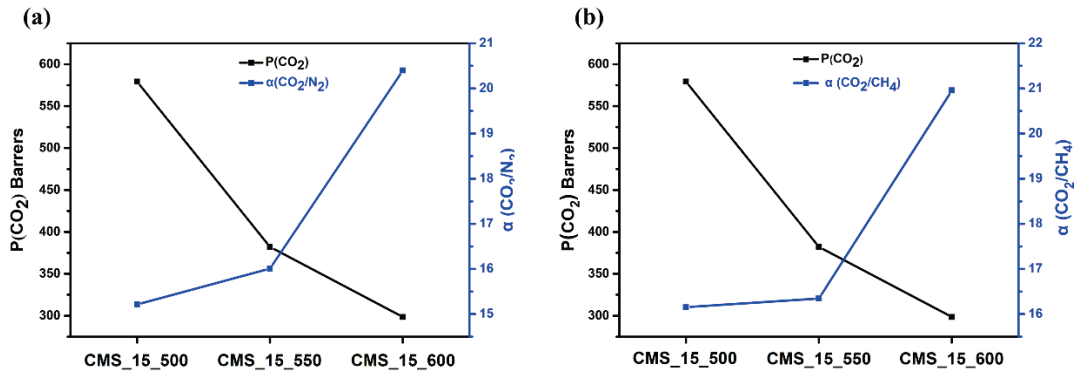

Fig. 5. The CO_2 permeability and selectivity of PVDF-derived CMSMs prepared at different pyrolysis temperature. (a) CO_2/N_2, (b) CO_2/CH_4.

CMS_15_500 had the highest CO_2 permeability of 579.31 barrers but the lowest CO_2/N_2 (15.21) and CO_2/CH_4 (16.15) selectivity among the three PVDF-derived CMSMs. Compared to CMS_15_500, CMS_15_600 exhibited the highest CO_2/N_2 (20.40) and CO_2/CH_4 (20.96) selectivity but the lowest CO_2 permeability of 298.51 barrers. As the pyrolysis temperature was increased, the permeability of all tested materials decreased, and the selectivity for CO_2/N_2 and CO_2/CH_4 increased; this occurred because the higher pyrolysis temperatures generated more tightly packed

366 carbon structures and shrinkage of the pore structure, as confirmed with proven by X-
367 ray diffraction (XRD), Raman and X-ray photoelectron spectroscopy (XPS), and this
368 decreased the gas permeability and improved the selectivity [49].

369 The performance of PVDF-derived CMS membranes was thoroughly evaluated
370 through a mixed gas separation test to provide valuable insights for practical
371 applications, and the results are presented in Fig. S8. The CO_2/CH_4 separation test
372 revealed increased CO_2 permeability from 579 Barrers to 779 Barrers and a rise in
373 CO_2/CH_4 selectivity from 16.15 to 47.86. This significant enhancement in selectivity
374 can be attributed to competitive adsorption due to the random carbonaceous tortuous
375 pathway. During the mixed gas flow, the preferential adsorption of CO_2 hinders the
376 adsorption of CH_4, resulting in lower CH_4 permeability—a phenomenon not observed
377 in single gas tests. The membrane's salient feature increases CO_2 permeability,
378 showcasing its potential for practical implementation in real-world scenarios.
379
380 *3.3. Aging Tests*
381 Aging tests were conducted to determine whether the as-prepared PVDF-derived
382 CMSMs can be utilized in realistic applications. The effects of physical/chemical aging
383 were investigated to determine whether aging provided more advantages for the as-
384 prepared PVDF-derived CMSMs. Thus, CMS_15_500 was chosen for the long-term
385 test because it had better CO_2 capture efficiency than the other samples. CMS_15_500
386 was stored at room temperature and 70% relative humidity to determine adaptability
387 for practical application. After aging for 31 days, thermal regeneration was executed by
388 implementing an identical pyrolysis process to accomplish performance recovery.
389 The results from the aging test of CMS_15_500 are shown in Fig. 6 and Table 1.

The CO_2 permeance gradually decreased during the 31 days due to the aging effect [50]. That is, self-retarding morphological rearrangements of the fresh CMSMs led to the more stable thermodynamic states that those of the fresh CMSMs, and a small amount of water vapor may have absorbed into the micropores of the CMSMs. Therefore, physical/chemical aging resulted in a decrease in the CO_2 permeance over time. However, typically, physical/chemical aging also causes an increase in selectivity due to shrinkage of the pore structure [51]. Thus, the performance of the aged CMSMs depended on a balance between decreasing permeance and increasing selectivity. In this case, CMS_15_500 showed a slight decrease in the CO_2 permeance from 234.88 barrers to 195.35 barrers with accompanying increases in the selectivity for CO_2/N_2 and CO_2/CH_4 at 31 days. The improved selectivity for CO_2/CH_4 was more apparent than that for CO_2/N_2 because of a significant loss in ultramicropores during physical aging but only a small loss for smaller molecules [52]. Thus, CMS_15_500 aged for 31 days had an extremely high selectivity for CO_2/CH_4 due to the larger difference in the kinetic diameters of CO_2 and CH_4. Regeneration of CMSMs by thermal treatment @500 degrees for membranes after 33 days of testing recovered the CO_2 permeance to almost 95%, being close to that of the fresh CMSM. The loss of CO_2 permeance was approximately 4% due to irreversible damage to the carbon structure via physical aging. In short, CMS_15_500 showed excellent carbon capture after being aged for 31 days, and the CO_2 permeability was recovered with a simple thermal regeneration procedure.

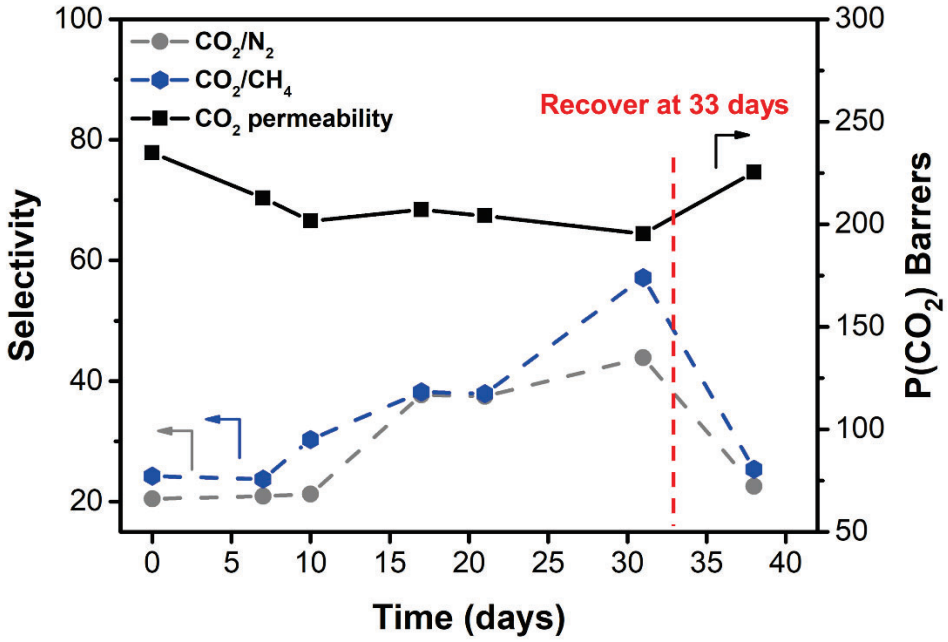

410

411 Fig. 6. Aging test diagram of CMS_15_500

412

413

414 Table 1. The single gas permeance and ideal selectivity of CMS_15_500 in the aging

415 test.

Hollow Fibers	P (GPU)			α	
	CO_2	N_2	CH_4	CO_2/N_2	CO_2/CH_4
Fresh	33.46	1.64	1.38	20.46	24.21
Aged (31 days)	27.83	0.63	0.49	43.86	57.14
After refresh	32.10	1.43	1.26	22.52	25.39

416

417

418

419

3.5. Literature Comparison

As the first supported hollow fiber carbon membrane and the first PVDF-derived CMSM for gas separation, the CMS_15_500 aged for 31 days exhibited promising performance for separation of CO_2/CH_4. A comparison of the CO_2/N_2 and CO_2/CH_4 performances of the supported carbon membrane and free-standing carbon membrane is shown in Fig. 7 and Table S2. As Fig. 7 shows, the CMS_15_500 aged for 31 days surpassed the 2008 Robeson upper bound for separation of CO_2/CH_4. PVDF-derived supported hollow fiber carbon membranes have ample potential for carbon capture and natural gas applications due to the readily available polymer precursors, simple and easy scale-up processes, high packing density of the hollow fiber membranes and better mechanical strength compared to those of free-standing CMSMs.

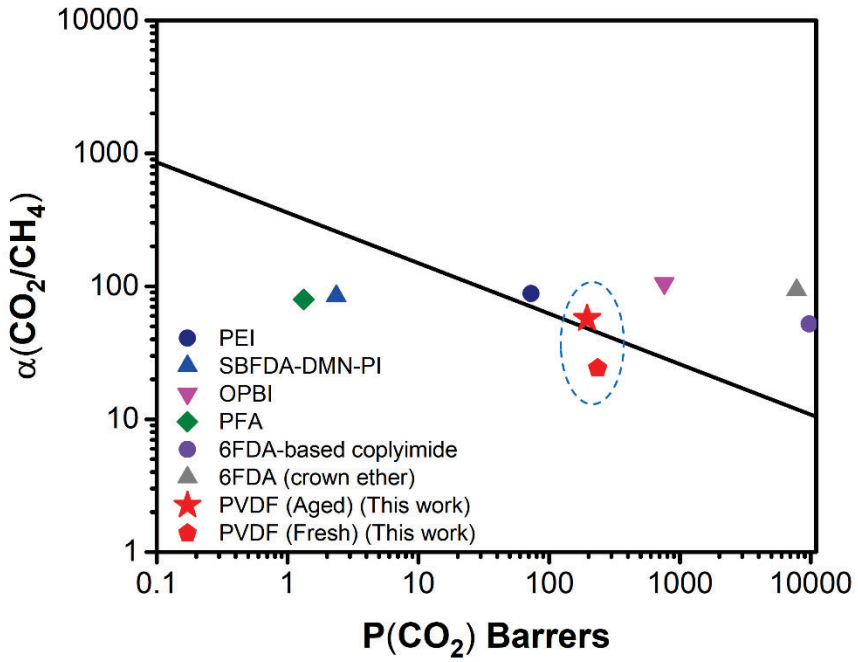

Fig. 7. Comparison of the gas separation performance of carbon membrane derived from different polymers [53-58].

4. Conclusions

In summary, the first defect-free PVDF-derived supported hollow fiber carbon membrane was fabricated for carbon capture without an intermediate layer. Dip-coating of the polymers over ceramics to develop the carbon membranes provides greater possibilities for practical applications. According to the characterization data, single pure gas permeation test and aging test, the following conclusions were drawn:

1. In-house alumina hollow fibers with precise pore sizes (200 nm), rough surfaces (R_a = 98 nm), and abundant -OH groups enabled uniform deposition of the PVDF solution.
2. A higher pyrolysis temperature led to a trade-off between improved selectivity and permeability of CO_2 due to the formation of a tighter carbon structure.
3. The as-prepared CMSMs were more resilient to aging, and CMS_15_500 aged for 31 days exhibited great separation performance (P_{CO2} = 195.35 barrers and CO_2/CH_4 = 57.14) for carbon capture and surpassed the 2008 Robeson upper bound.

5. Acknowledgments.

This work was financially supported by the National Science and Technology Council (NSTC) in Taiwan (Project number: 109-2221-E-002-102-MY3, 111-2622-E-002-005, NSTC 111-2634-F-002-016, and 111-2221-E-002-015-MY3), and Ministry of Education's Higher Education Sprout under the Feature Area Research Center Program (111L9006).

458 **References**

459 [1] W.J. Koros, G. Fleming, Membrane-based gas separation, Journal of membrane
460 science 83(1) (1993) 1-80.
461 [2] P. Pandey, R. Chauhan, Membranes for gas separation, Progress in polymer
462 science 26(6) (2001) 853-893.
463 [3] D.J. Harrigan, J. Yang, B.J. Sundell, J.A. Lawrence III, J.T. O'Brien, M.L. Ostraat,
464 Sour gas transport in poly (ether-b-amide) membranes for natural gas separations,
465 Journal of Membrane Science 595 (2020) 117497.
466 [4] C. Hepburn, E. Adlen, J. Beddington, E.A. Carter, S. Fuss, N. Mac Dowell, J.C.
467 Minx, P. Smith, C.K. Williams, The technological and economic prospects for CO_2
468 utilization and removal, Nature 575(7781) (2019) 87-97.
469 [5] J. Tong, L. Zhang, M. Han, K. Huang, Electrochemical separation of CO_2 from a
470 simulated flue gas with high-temperature ceramic–carbonate membrane: New
471 observations, Journal of Membrane Science 477 (2015) 1-6.
472 [6] B. Zhu, Y. Yang, K. Wang, X. He, B.H. Yin, L. Shao, Chemical topology
473 molecular engineering of CO_2-philic membranes toward highly efficient carbon
474 capture, Journal of Membrane Science 685 (2023) 121917.
475 [7] P. Su, S. Chen, L. Chen, W. Li, Constructing polymer/metal-organic framework
476 nanohybrids to design compatible polymer-filler-polymer membranes for CO_2
477 separation, Journal of Membrane Science 691 (2024) 122246.
478 [8] P.-C. Wu, H.-Y. Wang, D.-Y. Kang, K.-L. Tung, Green Delamination of 2D LDH
479 Nanosheets Incorporated in Mixed Matrix Membrane for CO_2 Capture, Journal of
480 Membrane Science (2024) 122797.
481 [9] H. Yuan, J. Liu, X. Zhang, L. Chen, Q. Zhang, L. Ma, Recent advances in
482 membrane-based materials for desalination and gas separation, Journal of Cleaner

Production (2023) 135845.
[10] D.-Y. Kang, J.S. Lee, Challenges in developing MOF-based membranes for gas separation, Langmuir 39(8) (2023) 2871-2880.
[11] H. Lopez-Marques, K.L. Gleason, M. Aguilar-Vega, R. Sulub-Sulub, J.E. Eichler, H. Oh, C.B. Mullins, B.D. Freeman, M. Kumar, Water vapor sorption and transport in carbon molecular sieve membranes, Journal of Membrane Science 691 (2024) 122170.
[12] Z. Dai, H. Guo, J. Deng, L. Deng, J. Yan, R.J. Spontak, Carbon molecular-sieve membranes developed from a Tröger's base polymer and possessing superior gas-separation performance, Journal of Membrane Science 680 (2023) 121731.
[13] J. Xin, X. Zhou, G. Huo, Z. Zhang, Y. Zhang, S. Kang, Z. Dai, N. Li, Development of high performance carbon molecular sieve membranes via tuning the side groups on PI precursors, Journal of Membrane Science 688 (2023) 122124.
[14] Y. Cao, K. Zhang, C. Zhang, W.J. Koros, Carbon molecular sieve hollow fiber membranes derived from dip-coated precursor hollow fibers comprising nanoparticles, Journal of Membrane Science 649 (2022) 120279.
[15] M. Hou, L. Li, Z. He, R. Xu, Y. Lu, J. Zhang, Z. Pan, C. Song, T. Wang, High-performance carbon molecular sieving membrane derived from a novel hydroxyl-containing polyetherimide precursor for CO_2 separations, Journal of Membrane Science 656 (2022) 120639.
[16] M. Hou, W. Qi, L. Li, R. Xu, J. Xue, Y. Zhang, C. Song, T. Wang, Carbon molecular sieve membrane with tunable microstructure for CO_2 separation: Effect of multiscale structures of polyimide precursors, Journal of Membrane Science 635 (2021) 119541.
[17] W. Ogieglo, T. Puspasari, A. Alabdulaaly, T.P.N. Nguyen, Z. Lai, I. Pinnau, Gas

508 separation performance and physical aging of tubular thin-film composite carbon
509 molecular sieve membranes based on a polyimide of intrinsic microporosity
510 precursor, Journal of Membrane Science 652 (2022) 120497.
511 [18] S. Liu, Z. Kang, L. Fan, X. Li, B. Zhang, Y. Feng, H. Liu, W. Fan, R. Wang, D.
512 Sun, Carbon molecular sieve membranes derived from hydrogen-bonded organic
513 frameworks for CO_2/CH_4 separation, Journal of Membrane Science 678 (2023)
514 121674.
515 [19] T. Araújo, G. Bernardo, A. Mendes, High-performance hydrogen separation
516 using cellulose-based carbon molecular sieve membranes, Journal of Membrane
517 Science 693 (2024) 122337.
518 [20] G. Liu, R. Li, X. Chen, L. Cheng, Y. Liu, G. Liu, W. Jin, Pyrolysis temperature-
519 regulated gas transport and aging properties in 6FDA-DAM polyimide-derived carbon
520 molecular sieve membranes, Separation and Purification Technology 313 (2023)
521 123459.
522 [21] L. Xu, M. Rungta, J. Hessler, W. Qiu, M. Brayden, M. Martinez, G. Barbay, W.J.
523 Koros, Physical aging in carbon molecular sieve membranes, Carbon 80 (2014) 155-
524 166.
525 [22] Z.-A. Chen, B. Zhao, J. Xin, Y. Liu, A new segment-level mixing strategy to
526 improve the gas separation performances of carbon molecular sieve membrane
527 derived from polymer blends, Journal of Membrane Science (2024) 122481.
528 [23] X. Chen, L. Wu, C. Xie, S. Xu, Y. Fan, N. Li, Small molecule DOPO-p-DP
529 crosslinked 6FDA-DAM-Br-85% carbon molecular sieve membrane with superior
530 aging for efficient gas separation, Journal of Membrane Science 687 (2023) 122072.
531 [24] J. Barsema, J. Balster, V. Jordan, N. Van der Vegt, M. Wessling, Functionalized
532 carbon molecular sieve membranes containing Ag-nanoclusters, Journal of membrane

533 science 219(1-2) (2003) 47-57.
534 [25] Z. Yang, W. Guo, H. Chen, T. Kobayashi, X. Suo, T. Wang, S. Wang, L. Cheng,
535 G. Liu, W. Jin, Benchmark CO_2 separation achieved by highly fluorinated nanoporous
536 molecular sieve membranes from nonporous precursor via in situ cross-linking,
537 Journal of Membrane Science 638 (2021) 119698.
538 [26] S. Poto, A. Aguirre, F. Huigh, M.A. Llosa-Tanco, D.A. Pacheco-Tanaka, F.
539 Gallucci, M.F.N. d'Angelo, Carbon molecular sieve membranes for water separation
540 in CO_2 hydrogenation reactions: Effect of the carbonization temperature, Journal of
541 Membrane Science 677 (2023) 121613.
542 [27] S.-J. Kim, J.F. Kim, Y.H. Cho, S.-E. Nam, H. Park, Y.-I. Park, Aging-resistant
543 carbon molecular sieve membrane derived from pre-crosslinked Matrimid® for
544 propylene/propane separation, Journal of Membrane Science 636 (2021) 119555.
545 [28] J.A. Lie, M.-B. Hägg, Carbon membranes from cellulose and metal loaded
546 cellulose, Carbon 43(12) (2005) 2600-2607.
547 [29] W. Qiu, F.S. Li, S. Fu, W.J. Koros, Isomer-tailored carbon molecular sieve
548 membranes with high gas separation performance, ChemSusChem 13(19) (2020)
549 5318-5328.
550 [30] H.B. Park, Y.K. Kim, J.M. Lee, S.Y. Lee, Y.M. Lee, Relationship between
551 chemical structure of aromatic polyimides and gas permeation properties of their
552 carbon molecular sieve membranes, Journal of Membrane Science 229(1-2) (2004)
553 117-127.
554 [31] N. Sazali, W.N.W. Salleh, A.F. Ismail, Y. Iwamoto, Incorporation of thermally
555 labile additives in polyimide carbon membrane for hydrogen separation, International
556 Journal of Hydrogen Energy 46(48) (2021) 24855-24863.
557 [32] A.K. Itta, H.-H. Tseng, Hydrogen separation performance of CMS membranes

derived from the imide-functional group of two similar types of precursors, international journal of hydrogen energy 36(14) (2011) 8645-8657.
[33] M.-Y. Wey, H.-H. Tseng, C.-k. Chiang, Effect of MFI zeolite intermediate layers on gas separation performance of carbon molecular sieve (CMS) membranes, Journal of membrane science 446 (2013) 220-229.
[34] C. Song, T. Wang, H. Jiang, X. Wang, Y. Cao, J. Qiu, Gas separation performance of C/CMS membranes derived from poly (furfuryl alcohol)(PFA) with different chemical structure, Journal of Membrane Science 361(1-2) (2010) 22-27.
[35] M. Rao, S. Sircar, Nanoporous carbon membranes for separation of gas mixtures by selective surface flow, Journal of Membrane Science 85(3) (1993) 253-264.
[36] J. Liu, E.M. Calverley, M.H. McAdon, J.M. Goss, Y. Liu, K.C. Andrews, T.D. Wolford, D.E. Beyer, C.S. Han, D.A. Anaya, New carbon molecular sieves for propylene/propane separation with high working capacity and separation factor, Carbon 123 (2017) 273-282.
[37] W.K. Cosey, K.J. Balkus Jr, J.P. Ferraris, I.H. Musselman, Reduced aging in carbon molecular sieve membranes derived from PIM-1 and MOP-18, Industrial & Engineering Chemistry Research 60(27) (2021) 9962-9970.
[38] J.G. Seong, J.C. Lewis, J.A. Matteson, E. Craddock, U. Martinez, H. Thakkar, A.D. Benavidez, K.A. Berchtold, R.P. Singh, Polybenzimidazole-derived carbon molecular sieve hollow fiber membranes with tailored oxygen selective transport, Carbon 192 (2022) 71-83.
[39] W. Wei, G. Qin, H. Hu, L. You, G. Chen, Preparation of supported carbon molecular sieve membrane from novolac phenol–formaldehyde resin, Journal of Membrane Science 303(1-2) (2007) 80-85.
[40] D. Kim, Y. Kwon, J.-H. Lee, S.-J. Kim, Y.-I. Park, Tailoring the Stabilization and

583 pyrolysis processes of carbon molecular sieve membrane derived from
584 polyacrylonitrile for ethylene/ethane separation, Membranes 12(1) (2022) 93.
585 [41] A.J. de Jesus Silva, M.M. Contreras, C.R. Nascimento, M.F. da Costa, Kinetics
586 of thermal degradation and lifetime study of poly (vinylidene fluoride)(PVDF)
587 subjected to bioethanol fuel accelerated aging, Heliyon 6(7) (2020).
588 [42] W.-Z. Huang, F. Lin, S.L. Lee, F.-T. Tao, K.-L. Tung, Fabrication of microporous
589 polyamide selective layer on macroporous ceramic hollow fibers via direct interfacial
590 polymerization for nanofiltration applications, Journal of Membrane Science 658
591 (2022) 120710.
592 [43] A. Jomekian, B. Bazooyar, S.A.A. Mansoori, Utilization and Comparison of
593 Different Food Wastes for the Synthesis of Two-Stage Activated Carbon-Based Mixed
594 Matrix Membranes for Gas Separation Applications, Waste and Biomass Valorization
595 (2023) 1-14.
596 [44] G. Wypych, 3-PVC MORPHOLOGY. PVC Degradation and Stabilization,
597 Boston: ChemTec Publishing, 2015.
598 [45] C.L. Beyler, M.M. Hirschler, Thermal decomposition of polymers, SFPE
599 handbook of fire protection engineering 2(7) (2002) 111-131.
600 [46] S. Reich, C. Thomsen, Raman spectroscopy of graphite, Philosophical
601 Transactions of the Royal Society of London. Series A: Mathematical, Physical and
602 Engineering Sciences 362(1824) (2004) 2271-2288.
603 [47] M.-Y. Wey, H.-H. Chen, Y.-T. Lin, H.-H. Tseng, Thin carbon hollow fiber
604 membrane with Knudsen diffusion for hydrogen/alkane separation: Effects of hollow
605 fiber module design and gas flow mode, International Journal of Hydrogen Energy
606 45(12) (2020) 7290-7302.
607 [48] H. Rajati, A.H. Navarchian, S. Tangestaninejad, Preparation and characterization

608 of mixed matrix membranes based on Matrimid/PVDF blend and MIL-101 (Cr) as
609 filler for CO_2/CH_4 separation, Chemical Engineering Science 185 (2018) 92-104.
610 [49] S. Fu, G.B. Wenz, E.S. Sanders, S.S. Kulkarni, W. Qiu, C. Ma, W.J. Koros,
611 Effects of pyrolysis conditions on gas separation properties of 6FDA/DETDA: DABA
612 (3: 2) derived carbon molecular sieve membranes, Journal of Membrane Science 520
613 (2016) 699-711.
614 [50] Y. Zhang, M. Sun, L. Li, R. Xu, Y. Pan, T. Wang, Carbon molecular sieve/ZSM-5
615 mixed matrix membranes with enhanced gas separation performance and the
616 performance recovery of the aging membranes, Journal of Membrane Science 660
617 (2022) 120869.
618 [51] S.S. Hays, O. Sanyal, N.E. León, P. Arab, W.J. Koros, Envisioned role of slit
619 bypass pores in physical aging of carbon molecular sieve membranes, Carbon 157
620 (2020) 385-394.
621 [52] Z. Liu, W. Qiu, W.J. Koros, New Insights into Physical Aging-Induced Structure
622 Evolution in Carbon Molecular Sieve Membranes, Angewandte Chemie International
623 Edition 61(45) (2022) e202210831.
624 [53] H.-H. Tseng, C.-T. Wang, G.-L. Zhuang, P. Uchytil, J. Reznickova, K.
625 Setnickova, Enhanced H_2/CH_4 and H_2/CO_2 separation by carbon molecular sieve
626 membrane coated on titania modified alumina support: Effects of TiO2 intermediate
627 layer preparation variables on interfacial adhesion, Journal of Membrane Science 510
628 (2016) 391-404.
629 [54] C. Song, T. Wang, J. Qiu, Preparation of C/CMS composite membranes derived
630 from Poly (furfuryl alcohol) polymerized by iodine catalyst, Desalination 249(2)
631 (2009) 486-489.
632 [55] W. Jiao, Y. Ban, Z. Shi, X. Jiang, Y. Li, W. Yang, Gas separation performance of

633 supported carbon molecular sieve membranes based on soluble polybenzimidazole,
634 Journal of Membrane Science 533 (2017) 1-10.
635 [56] M. Teixeira, S.C. Rodrigues, M. Campo, D.A.P. Tanaka, M.A.L. Tanco, L.M.
636 Madeira, J.M. Sousa, A. Mendes, Boehmite-phenolic resin carbon molecular sieve
637 membranes—Permeation and adsorption studies, Chemical Engineering Research and
638 Design 92(11) (2014) 2668-2680.
639 [57] D. Wu, X. Qu, X. He, C. Yi, B. Zhang, B. Yang, High-Performance Carbon
640 Molecular Sieve Membrane Derived from a Crown Ether-Containing Co-Polyimide
641 Precursor for Gas Separation, Industrial & Engineering Chemistry Research (2023).
642 [58] Z. Liu, W. Qiu, W. Quan, W.J. Koros, Advanced carbon molecular sieve
643 membranes derived from molecularly engineered cross-linkable copolyimide for gas
644 separations, Nature Materials 22(1) (2023) 109-116.
645